Accurate Elucidation of Oxidation Under Heavy Ozone Pollution: A Full Suite of Radical Measurement In the Chemical-complex Atmosphere

Renzhi Hu[1], Guoxian Zhang[1,2,×], Haotian Cai[1], Jingyi Guo[1], Keding Lu[4], Xin Li[4], Shengrong Lou[5], Zhaofeng Tan[4], Changjin Hu[1], Pinhua Xie[1,3,××], Wenqing Liu[1,3]

[1] Key Laboratory of Environment Optics and Technology, Anhui Institute of Optics and Fine Mechanics, HFIPS, Chinese Academy of Sciences, Hefei, China

[2] School of Physics and New Energy, Xuzhou University of Technology, Xuzhou, China

[3] College of Resources and Environment, University of Chinese Academy of Science, Beijing, China

[4] State Key Joint Laboratory of Environmental Simulation and Pollution Control, College of Environmental Sciences and Engineering, Peking University, Beijing, China

[5] State Environmental Protection Key Laboratory of the Formation and Prevention of Urban Air Pollution Complex, Shanghai Academy of Environmental Sciences, Shanghai, China

×**Correspondence to:** Guoxian Zhang, School of Physics and New Energy, Xuzhou University of Technology, Xuzhou, China

××**Correspondence to:** Pinhua Xie, Key Laboratory of Environment Optics and Technology, Anhui Institute of Optics and Fine Mechanics, HFIPS, Chinese Academy of Sciences, Hefei, China

Email addresses: gxzhang@aiofm.ac.cn (Guoxian Zhang); phxie@aiofm.ac.cn (Pinhua Xie)

Abstract: The Yangze River Delta (YRD) in China encountered with prolonged ozone pollution in September 2020. To accurately elucidate the limitations of oxidation processes in the chemical-complex atmosphere, a full suite of radical measurements (OH, HO_2, RO_2, and k_{OH}) was established in YRD region for the first time. The diurnal peaks of radicals exhibited considerable variation due to environmental factors, showing ranges of 3.6 to 27.1×10^6 cm^{-3} for OH, 2.1 to 33.2×10^8 cm^{-3} for HO_2, and 4.9 to 30.5×10^8 cm^{-3} for RO_2. The simulated results provided by the RACM2-LIM1 mechanism failed to adequately match the observed data both in radical concentration and experimental budget at a heavy ozone pollution episode. Sensitivity tests utilizing a comprehensive set of radical measurements revealed that the higher aldehyde mechanism (HAM) effectively complements the regeneration of OH radicals, yielding enhancements of 4.4% - 6.0% compared to the base scenario, while the concentrations of HO_2 and RO_2 radicals have shown increments of about 7.4% and 12.5%, respectively. It is noteworthy that under the constraints of k_{OH} measurement, the inclusion of OVOCs and larger alkoxy radicals derived from monoterpenes improved the model-measurement consistency for ozone formation, reducing the discrepancy under high NO conditions from 4.17 to 2.39. This outcome corroborates the hypothesis of sensitivity analysis as it pertains to ozone formation. Moving forward, by implementing a comprehensive radical detection approach, further investigations should concentrate on a broader range of OVOCs to rectify the imbalance associated with RO_2 radicals, thereby providing a more precise understanding of oxidation processes during severe ozone pollution episodes.

Keywords: FAGE-LIF; Full-chain detection; Radical; P(Ox); OVOCs;

1 Introduction

In recent years, China's rapid economic development has led to severe environmental pollution problems, which significant impacted the respiratory, dermatological, and visual health of local residents (Wang et al., 2022c; Huang et al., 2018). This has raised concerns about the coexistence of regional primary and secondary pollution, making air quality improvement efforts a focal point (Liu et al., 2021; Wang et al., 2022a). In the complex atmosphere, near-surface ozone (O_3) is formed through continuous photochemical reactions between nitrogen oxides ($NOx \equiv NO+NO_2$) and volatile organic compounds (VOCs) under light conditions, while hydroxyl radicals (OH) serve as the main oxidant in the troposphere, converting VOCs into hydroperoxy (HO_2) and organic peroxy (RO_2) radicals (Rohrer et al., 2014; Hofzumahaus et al., 2009). Additionally, the oxidation of nitric oxide (NO) and peroxy radicals produce nitrogen dioxide (NO_2), which is the sole photochemical source of ozone (Lu et al., 2012; Stone et al., 2012).

Despite numerous experimental and theoretical explorations to establish the radical-cored photooxidation mechanism in the troposphere, field observations were primarily focused on HOx ($HOx \equiv OH + HO_2$) radicals due to the limitations of detection technology (Kanaya et al., 2012; Lu et al., 2012; Hofzumahaus et al., 2009; Yugo Kanaya and Tanimoto, 2007; Ren et al., 2008; Stone et al., 2012; Levy, 1971). Recent advancements in detection technology, such as the application of a new LIF technique (ROxLIF), have made the detection of RO_2 radicals possible (Whalley et al., 2013; Tan et al., 2017a). Moreover, the union of comprehensive field campaigns and box model, has proven to be an effective method for verifying the integrity of radical chemistry at local to global scales (Lu et al., 2019b; Tan et al., 2018). Several experiments have indicated that the existing atmospheric chemical mechanism posted challenges in deepening the understanding of the regional pollution explosion (Whalley et al., 2021; Slater et al., 2020; Tan et al., 2017a; Woodward-Massey et al., 2023). For instance, the observation of up to 4×10^9 cm^{-3} of RO_2 radical in the center of Beijing in 2017 (APHH) was significantly underestimated by the MCM v3.3.1 mechanism (Whalley et al., 2021). Further exploring the unreproducible concentration and the oxidation process in the chemical-complex atmosphere is deemed necessary (Whalley et al., 2021; Woodward-Massey et al., 2023).

The YRD region, situated between the North China Plain (NCP) and Pearl River Delta (PRD), is highly prone to regional transport interactions and aerosol-boundary layer feedback (Jia et al., 2021; Huang et al., 2020). In an effort to gain a better understanding between the complex radical chemistry and the intensive oxidation level in the Yangze River Delta, TROPSTECT-YRD (The experiment on Radical chemistry and Ozone Pollution perSpectively: long-Term Elucidation of the photochemiCal oxidaTion in the Yangze River Delta) was conducted in Hefei during September 2020. Accurate elucidation of the oxidation process under heavy ozone pollution was provided by a full suite of radical measurement (OH, HO_2, RO_2 and k_{OH}) in the chemical-complex atmosphere.

2 Materials and methods

2.1 Site description and instrumentation

The TROPSTECT observation was conducted from 1 to 20 September 2020 at the Science Island background station (31.9° N, 117.2°E) in Hefei, a typical megacity located in the central region of Anhui Province within the Yangtze River Delta. The station is situated on a peninsula with abundant vegetation to the northwest of urban areas and is in close proximity to Dongpu Lake, which is only 200 meters away, and the main road, positioned 250 meters southward (Fig. 1). Consequently, the relatively enclosed environment exhibits typical suburban characteristics of anthropogenic emissions. The station is located in the transition region between urban and suburban areas, reflecting the regional transpor of pollution in Hefei and its surrounding areas.

Fig. 1. (a) The location of the measurement site (source: © Google Earth).
(b) The close shot of the measurement site location (source: © Google Earth).
(c) The actual image for the LIF-Box.

Regarding the instrumentation, a group of oxidation-related instruments were installed on the 7th floor of the Comprehensive Building at the Anhui Institute of Optics and Fine Mechanics (AIOFM), with all sampling outlets positioned more than 20 meters above the ground. The details of the instruments measuring various parameters such as meteorological factors (WS, WD, T, RH, P, Jvalues), gas pollutants (O_3, CO, SO_2, NO, NO_2, HONO, HCHO, PAN), and non-methane hydrocarbons (NMHCs) are provided in Table S1.

The measurement of NO, NO_2, O_3, CO, and SO_2 was carried out using commercial Thermo Electron model series instruments. Thereof, NO and NO_2 were measured using a chemical luminescence method (CL) with an enhanced trace-level NO-NO_2-NOx analyzer (PKU-PL), which achieved a detection limit of 50 ppt (Tan et al., 2017a). The detection of O_3 and SO_2 was conducted through Thermo Electron model 49i and 43i, respectively, while Thermo Electron model 48i was utilized for CO detection. Cavity ring-down spectroscopy (CRDS, Picarro-G2401) was employed for CO detection in parallel, and another ultraviolet absorption instrument (Ecotech EC9810B) was for ozone detection. The instrument inlets were placed within 5 meters of each other for comparison.

All Thermo series gas analyzers were equipped with individual sampling inlet tubing, which was made of Polyfluoroalkoxy (PFA, with 6.35 mm outer-diameter), and the flow rate was operated at 1.5 L/min. The total length of the inlet tubing from the sampling tip to the instrument inlet was 2.5 m, with the entire line wrapped with insulation material to prevent condensation of water vapor. To ensure measurement accuracy, the instruments in the campaign underwent zero point calibration procedures during the early (August 31st) and late (September 21st) observation periods. Furthermore, additional zero calibration for Thermo 48i CO detection was undertaken daily from 0:00-0:30 to minimize shift correction. Zero-point calibration includes the instrument and the complete inlet system. Cross-calibrations for O_3 and CO measurements were carried out during the middle (September 9th). The comparison results revealed high consistency within the instrument accuracy range for both CO and O_3 measurements (Fig. S1(a)(b)).

HONO was detected using a home-built instrument by cavity-enhanced absorption spectroscopy (CEAS), while formaldehyde was determined by the Hantzsch method (SDL MODEL 4050) (Duan et al., 2018; Yang et al., 2021a). An automated gas chromatograph equipped with a mass spectrometer and flame ionization detector

(GC-FID/MS) was employed for the online measurement of 99 VOCs species. Information table for parts of the VOC monitoring species by online GC-MS/FID was listed in Table S2.

The eight crucial photolysis frequencies (j(NO_2), j(H_2O_2), j(HCHO_M), j(HCHO_R), j(HONO), j(NO_3_M), j(NO_3_R), j(O^1D)) were directly measured by a photolysis spectrometer (Metcon, Germany). The unmeasured photolysis frequencies of the remaining active species were computed using Eq.(1):

$$j = l \cdot cos(\chi)^m \cdot e^{-n \cdot sec(\chi)} \tag{1}$$

The variations in photolysis frequency due to solar zenith angle (χ) were adjusted based on the ratio of observed and simulated j(NO_2). The optimal values for parameters (l, m, and n) for different photolysis frequencies were extensively detailed by the MCM v3.3.1 (http://mcm.york.ac.uk/parameters/photolysis_param.htt) (Jenkin et al., 2003; Jenkin et al., 1997).

2.2 Radical measurement

2.2.1 OH, HO_2, RO_2 Concentrations

The laser-induced fluorescence instrument developed by the Anhui Institute of Optics and Fine Mechanics (AIOFM-LIF) was used to simultaneously detect the concentrations of OH, HO_2, and RO_2 radicals, along with OH reactivity (k_{OH}). The OH radical was directly measured by detecting on-resonance fluorescence excited by a 308 nm laser. An indirect measurement for HO_2 was carried out after converting it to OH at a fixed efficiency (Heard and Pilling, 2003).

The laser utilized for fluorescence excitation is a high-frequency tunable dye laser that emits a 308 nm laser, with the laser power divided into a ratio of 0.45:0.45:0.08:0.02. Of this power, 90% is directed towards fluorescence cells for concentration and reactivity detection via optical fibers, respectively. 8% of the laser power is directed to a reference cell, while the remaining 2% is used to monitor real-time power fluctuations. The laser is transmitted through HO_2, OH, and RO_2 cells in turn via a coaxial optical path. Two photodiodes are set up at the end of the reference cell and RO_2 detection cell, respectively. The voltage signals and power fluctuations are compared synchronously to diagnose the laser stability. To maintain detection efficiency, the power inside the measurement cells should not be less than 10 mW. Sampling nozzles of 0.4 mm are deployed above OH and

HO_2 cells for efficient sampling at a flow rate of approximately 1.1 SLM, and the pressure for all fluorescence cells are maintained at 400 Pa. The micro-channel plate (MCP) detects the weak fluorescence signal collected by lens systems with low noise and high gain. Additionally, a digital delay generator (DG645) optimizes the timing control between the laser output, signal detection, and data acquisition. All of these modules are integrated into a sampling box with constant air conditioning, except for the laser.

The detection of RO_2 radicals is more complex compared to the integrated detection of OH and HO_2 radicals (Whalley et al., 2013). To achieve the complete chemical conversion from ROx to HO_2, a crucial role is played by a 66 mm×830 mm aluminium flow tube, whose performance has been confirmed through the CHOOSE-2019 field campaign (Li et al., 2020). A mixture of 0.17% CO and 0.7 ppm NO injected into the flow tube facilitates the reduction of heterogeneous radical loss and enhancement of conversion efficiency. The sampling flow is limited to 7 SLM by a 1 mm nozzle, and the tube pressure is maintained at 25 hPa. In contrast to the HOx cells, the large-diameter nozzle (4 mm) is equipped above the cell, and a high concentration of NO (~300 ppm) facilitates the full magnitude $HO_2 \rightarrow OH$ conversion.

The observation data (H_2O, O_3) is combined with experimental characterization to eliminate ozone photolysis interference, and most interference signals are excluded by utilizing wavelength modulation (Zhang et al., 2022a). A comparison experiment with PKU-LIF demonstrated the consistency of OH measurement in complex atmosphere (Zhang et al., 2022b). An additional atmospheric oxidation observation was conducted in the same location and season in 2022 with a chemical modulation method to determine the chemical background of OH radicals (Fig. S2). During the ozone pollution (2022.9.29-2022.10.3), the daytime peaks of ozone concentration above 75 ppb, accompanied by alkene species approaching ~10 ppb. The diurnal concentration of isoprene was also a high level (>1 ppb). The chemical conditions are more favourable to induce OH interference than in the TROPSTECT campaign, while the OH concentrations achieved by chemical modulation (OH_{chem}) and wavelength modulation (OH_{wav}) were in good agreement. No obvious chemical background was observed by deploying an inlet pre-injector. While it was not anticipated that OH measurements would be influenced by internal interference, the possibility of unknown interferences cannot be excluded since titration tests were not employed during the campaign. Consequently, the OH measurements represent an upper bound to the actual values.

For HO_2 measurement, lower NO concentration (~1.6×10^{12} cm^{-3}, corresponding to ~15% conversion efficiency) are selected to limit the $RO_2 \rightarrow HO_2$ interference to less than 5% (Wang et al., 2021). Since only the total-RO_2 mode is used for the campaign, the additional uncertainty introduced by RO_2/$R(OH)O_2$ classification is negligible (Tan et al., 2017b). The observed maximum daily PAN (11:00-14:00) is only 1.15±0.67 ppb, resulting in a calculated PAN-pyrolytic interference for RO_2 measurement of less than 1 ppt (Fuchs et al., 2008). The general applicability of AIOFM-LIF in complex atmosphere has been demonstrated through various campaigns (Zhang et al., 2022b; Wang et al., 2021; Wang et al., 2019a).

To complete the calibration task, a standard source stably generates equal amounts of OH and HO_2 radicals (Wang et al., 2020). The radical source is also capable of yielding specific RO_2 by titrating hydrocarbon with OH. It is noteworthy that CH_3O_2 has the highest mixing ratio in the RO_2 species, thus it was chosen to represent for sensitivity calibration. The instrument is calibrated every two days, except during rainy weather. The limit of detection (LOD) for OH, HO_2, and RO_2 in different cells with a typical laser power of 10 mW is measured at 3.3×10^5 cm^{-3}, 1.1×10^6 cm^{-3}, and 2.5×10^6 cm^{-3}, respectively (60 s, 1σ). Measurement accuracy for OH, HO_2, and RO_2 radicals are reported to be 13%, 17%, and 21%, respectively.

2.2.2 OH reactivity(k_{OH})

The detection of k_{OH} in the atmosphere, defined as the reciprocal of OH lifetime, was conducted using a laser flash photolysis laser-induced fluorescence (LP-LIF) instrument (Lou et al., 2010). The configuration structure for k_{OH} measurement has been detailed in a previous study(Liu et al., 2019). The flow tube in the OH production-reaction unit is at ambient pressure, with a gas flow rate of 17 SLM. A pulsed laser beam (266 nm with an average power of 15 mJ) is output from a frequency-quadrupled Nd:YAG laser, which generates stable OH radical through flash photolysis of ambient ozone in the flow tube. Consistent and stable production of OH radicals is ensured by maintaining a stable concentration of reactants, flow field, and laser energy. Under conditions of 80 ppb O_3 and 8000 ppm water vapor concentration, OH radicals produced in the flow tube remains at the concentration order of 10^9 cm^{-3}. Subsequently, the OH radicals are sampled through a nozzle into a fluorescence cell. The OH fluorescence signal is then detected using laser pump and probe techniques and is fitted to calculate the slope of OH decay (k_{OH}). The detection accuracy, achieved with an integration time of 180 s, is 0.3 s^{-1} (1σ).

2.3 Observation-Based Model

The Regional Atmospheric Chemical Mechanism version 2 (RACM2) incorporating the latest Leuven isoprene mechanism (LIM) was utilized to simulate the concentrations and reactions of OH, HO_2, and RO_2 radicals (Stockwell et al., 1997; Griffith et al., 2013; Peeters et al., 2014). The RACM2-LIM1 mechanism was specifically involved with fewer species compared to the explicit MCM mechanism, thus ensuring higher operational efficiency (Liu et al., 2022). The comprehensive list of model constraints was provided in Table S3. The measured NMHCs include 29 alkanes, 11 alkenes, 15 aromatics, as well as acetylene and isoprene. For the base scenario, boundary conditions were established using the observed species, with assumed concentrations of hydrogen (H_2) and methane (CH_4) at 550 ppb and 1900 ppb, respectively. An ozone-simulation test was conducted to determine the suitable depositional lifetime (τ_D) for the species involved in the base model. At the lifetime of 24 hours, with a corresponding first-order loss rate of 1.1 cm/s (assuming a boundary layer height of 1 km), the simulated ozone concentration closely matched the observed values (Fig. S3). The time resolution of all constraints was uniformly set to 15 minutes through averaging or linear interpolation. To reinitialize unconstrained species to a steady-state, three days of data were input in advance as the spin-up time.

To improve the model-measurement consistency between OH, HO_2 and RO_2 radicals, a series of sensitivity analyses were performed to evaluate the impacts of potential mechanisms, as detailed in Table 1. The HAM mechanism was introduced to discuss the influence of reactive aldehyde chemistry, and additional monoterpene species (MTS) was employed to represent the complex isomerization steps experienced by RO_2 radicals derived from other unmeasured VOCs. Reactions involving monoterpene and HAM mechanism have been listed in Table S4&S5. Furthermore, under the framework of the base model, another investigation on the photochemical role of unmeasured OVOCs species in the atmosphere was conducted by the MCM v3.3.1 mechanism.

Table.1. The sensitive test scenarios utilized to improve the model-measurement consistency between OH, HO_2 and RO_2 radicals.

Scenario	Configuration	Purpose
Base	RACM2 updated with isoprene reaction scheme (LIM)	The base case with the species involved in Table S3 are constrained as boundary conditions.
MCM on	As the base scenario, but the reaction scheme was replaced by the MCM v3.3.1 mechanism .	To assess the photochemical role of unmeasured OVOCs species in the atmosphere.
HAM on (4 × ALD)	As the base scenario, but add the reactive aldehyde chemistry, and the concentration of ALD was amplified by a factor of 4.	To quantify the impact of missing aldehyde primary emissions on ROx chemistry.
HAM on (4 × ALD+MTS)	As the HAM on (4 × ALD) scenario, but add a monoterpene source, and the monoterpene level is ~0.4 ppb.	Utilizing monoterpene-derived RO_2 to represent the alkoxy radicals with rather complex chemical structures.
Ozone simulation	As the base scenario, but remove the constraints of the observed ozone and NO concentrations.	To test the suitable lifetime for the base model.
HCHO simulation	As the base scenario, but remove the constraint of the observed HCHO concentration.	To test the simulation effect of the existing mechanism on formaldehyde concentration.

The local formation of ozone can be accurately quantified through the online measurement of ROx radicals (Tan et al., 2018). To overcome the interference from NO, the total oxidant (Ox), which is defined as the sum of NO_2 and O_3, can serve as a reliable parameter to indicate the level of oxidation. Eq.(2) shows that the rate of NO oxidation by peroxy radicals is equivalent to the production of O_3, denoted as F(Ox):

$$F(O_x) = k_{HO_2+NO}[NO][HO_2] + \sum_i k_{RO_2^i+NO}[NO]RO_2^i \tag{2}$$

The major loss pathways for Ox encompass ozone photolysis, ozonolysis reactions, and radical-related reactions (OH/HO_2+O_3, OH+NO_2), represented as D(Ox) in Eq.(3):

$$D(O_x) = \varphi_{OH} j(O^1D)[O_3] + \Sigma i \left\{\varphi_{OH}^i k_{Alkenes+O_3}^i [Alkenes][O_3]\right\} + (k_{O_3+OH}[OH] + k_{O_3+HO_2}[HO_2])[O_3] + k_{OH+NO_2}[OH][NO_2] \tag{3}$$

Here, the OH yields from ozone photolysis and ozonolysis reactions are denoted as φ_{OH} and φ_{OH}^i, respectively.

The net photochemical Ox production rate in the troposphere, denoted as P(Ox) in Eq.(4), can therefore be calculated as the difference between Eqs. (2) and (3):

$$P(O_x) = F(O_x) - D(O_x) \tag{4}$$

2.4 Experimental budget analysis

In this study, an experimental radical budget analysis was also conducted (Eqs. (5) - (12)). Unlike model studies, this method relies solely on field measurements (concentrations and photolysis rates) and chemical kinetic data, without depending on concentrations calculated by models(Whalley et al., 2021; Tan et al., 2019b). Given the short-lived characteristics of OH, HO_2, and RO_2 radicals, it is expected that the concentrations are in a steady state, with total production and loss rates being balanced(Lu et al., 2019a). By comparing the known sources and sinks for radicals, unknown processes for initiation, transformation and termination can be determined.

$$\begin{aligned} P(OH) = {} & j_{HONO}[HONO] + \varphi_{OH} j(O^1D)[O_3] + \Sigma i\left\{\varphi^i_{OH} k^i_{Alkenes+O_3}[Alkenes][O_3]\right\} \\ & + (k_{HO_2+NO}[NO] + k_{HO_2+O_3}[O_3])[HO_2] \end{aligned} \tag{5}$$

$$D(OH) = [OH] \times k_{OH} \tag{6}$$

$$\begin{aligned} P(HO_2) = {} & 2 \times j_{HCHO\_R}[HCHO] + \Sigma i\left\{\varphi^i_{HO_2} k^i_{Alkenes+O_3}[Alkenes][O_3]\right\} \\ & + (k_{HCHO+OH}[HCHO] + k_{CO+OH}[CO])[OH] \\ & + \alpha k_{RO_2+NO}[NO][RO_2] \end{aligned} \tag{7}$$

$$\begin{aligned} D(HO_2) = {} & (k_{HO_2+NO}[NO] + k_{HO_2+O_3}[O_3] + k_{HO_2+RO_2}[RO_2] \\ & + 2 \times k_{HO_2+HO_2}[HO_2])[HO_2] \end{aligned} \tag{8}$$

$$\begin{aligned} P(RO_2) = {} & \Sigma i\left\{\varphi^i_{RO_2} k^i_{Alkenes+O_3}[Alkenes][O_3]\right\} \\ & + k_{OH}[VOCs][OH] \end{aligned} \tag{9}$$

$$\begin{aligned} D(RO_2) = {} & \left\{(\alpha + \beta) k_{RO_2+NO}[NO] + (2 \times k_{RO_2+RO_2}[RO_2] \right. \\ & \left. + k_{HO_2+RO_2}[HO_2])\right\}[RO_2] \end{aligned} \tag{10}$$

$$\begin{aligned} P(RO_x) = {} & \Sigma i\left\{(\varphi^i_{OH} + \varphi^i_{HO_2} + \varphi^i_{RO_2}) k^i_{Alkenes+O_3}[Alkenes][O_3]\right\} + j_{HONO}[HONO] \\ & + \varphi_{OH} j(O^1D)[O_3] + 2 \times j_{HCHO\_R}[HCHO] \end{aligned} \tag{11}$$

$$\begin{aligned} D(RO_x) = {} & (k_{OH+NO_2}[NO_2] + k_{OH+NO}[NO])[OH] + \beta k_{RO_2+NO}[NO] \\ & + 2 \times (k_{RO_2+RO_2}[RO_2][RO_2] + k_{HO_2+RO_2}[HO_2][RO_2] \\ & + k_{HO_2+HO_2}[HO_2][HO_2]) \end{aligned} \tag{12}$$

In which, j(HONO), $j(O^1D)$ are the measured photolysis rates of HONO and O_3, respectively, and jHCHO_R is the measured photolysis rate for the channel of formaldehyde photolysis generating HO_2. φ_{OH} represent the OH yield in the O_3 photolysis reaction. φ^i_{OH}, $\varphi^i_{HO_2}$ and $\varphi^i_{RO_2}$ are the yields for the ozonolysis reaction producing OH, HO_2, and RO_2, respectively. α is the proportion of RO_2 radicals reacting with NO that are converted to HO_2, and β is the proportion of alkyl nitrates formation, which are set to 1 and 0.05, respectively(Tan et al., 2019b).

3 Results

3.1 Overview of Measurement

During the observation period, the meteorological parameters and trace gas concentrations were plotted in Fig. S4. The timeseries revealed that the peak temperature exceeded 30°C, and the humidity levels remained between 30 – 50% during the daytime. The photolysis rates were observed to peak at noon (11:00 – 13:00), with $j(O^1D)$ and $j(NO_2)$ reaching approximately 3×10^{-5} s^{-1} and 8×10^{-3} s^{-1}, respectively. Brief rainfall events temporarily happened on September 10th, 15th, and 17th, but totally favorable meteorologies induced the prolonged ozone pollution. The daily maximum 8-hour average ozone concentration (MDA8), as depicted in Fig. 2, consistently exceeded the Chinese Grade I national air quality standard (GB3095-2012) throughout the observation, with nine days exceeding the Grade II standard.

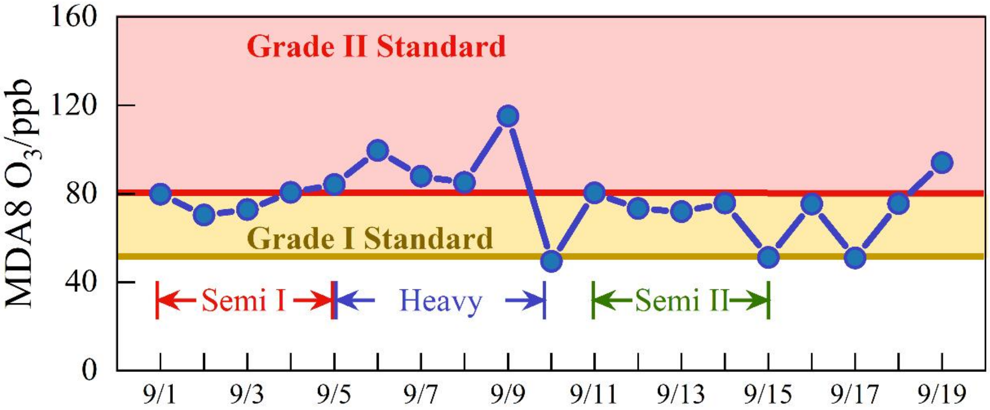

Fig. 2. The daily maximum 8 h average O_3 during the campaign. The yellow and red lines denote the Grade I and Grade II national standards for O_3, respectively. Brief rainfall events temporarily happened on10, 15, and 17 Sep.

The ozone pollution can be categorized into three continuous periods based on pollution levels, which disclose transitional 'Semi - Heavy - Semi' pollution characteristics. Fig. 3 depicts daily variations in meteorological and trace gas concentrations for different periods. During the Semi I (1 to 5 September) and Semi II (11 to 14 September) periods, the MDA8 levels exceeded Grade I standard, with an average value of 75.92±5.14 ppb and 75.45±3.73 ppb, respectively. Notably, NO levels peaked around 9:00 and rapidly decreased to a few hundred ppt due to photochemistry. In addition, HONO and NO_2 exhibited bimodal variations, with diurnal concentration ranges of 0.09 – 0.50 ppb and 3.35 – 13.77 ppb, respectively. The HONO/NO_2 ratios during both Semi periods were consistent with previous urban/suburban observations, with daytime values of 0.049±0.014 and 0.035±0.012, respectively (Yang et al., 2021b; Shi et al., 2020; Hu et al., 2022). Isoprene levels accumulated during the day and decreased at night during both Semi pollution episodes, with a diurnal average concentration in Semi II only 49.3% of that in Semi I (0.71±0.087 ppb vs 0.35±0.073 ppb). Formaldehyde, as the key oxidation species, exhibited a concentration profile mirroring that of isoprene, with significantly higher concentrations ranging from 1.20 to 36.34 ppb compared to other urban regions (Ma et al., 2022; Yang et al., 2022; Tan et al., 2017b; Yang et al., 2021a). Heavy pollution episodes from 5 to 9 September resulted in daytime ozone concentration as high as 129.9 ppb, and oxidation-related species such as HCHO, HONO, NOx, and VOCs increased synchronously compared to other days.

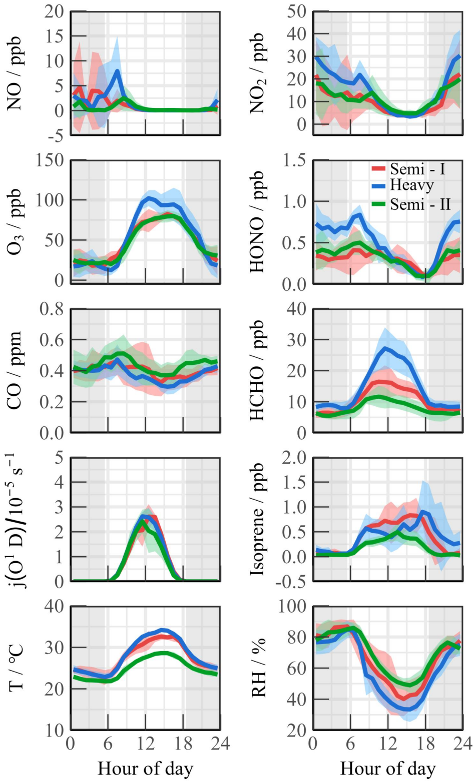

Fig. 3. Mean diurnal profiles of observed meteorological and chemical parameters during the campaign. Three periods were divided for subsequent study (Semi I, Heavy, and Semi II).

3.2 ROx radical concentrations and budgets

The observed and modeled timeseries for OH, HO_2, RO_2, and k_{OH} during the observation time are depicted in Fig. 4. The diurnal peaks of radicals exhibited a wide span due to changes in environmental conditions, with ranges of 3.6 – 27.1×10^6 cm^{-3} for OH, 2.1 – 33.2×10^8 cm^{-3} for HO_2, and 4.9 – 30.5×10^8 cm^{-3} for RO_2. Continuous data for

k_{OH} observation were acquired within a range of 8.6 – 30.2 s^{-1}. Fig. S5 presents the diurnal profiles of the observed and modeled values during different episodes. The diurnal maximum of OH radical at noon differed between Semi I and Semi II, with 9.28×10^6 cm^{-3} and 5.08×10^6 cm^{-3}, respectively, while total peroxy radicals (HO_2+RO_2) remained at similar levels with 19.43×10^8 cm^{-3} and 18.38×10^8 cm^{-3}. Additionally, the distribution of peroxy radicals are not similar in the two Semi periods, with HO_2/RO_2 ratios of 1.69:1 and 0.76:1, respectively, which reflects the uneven oxidation levels between Semi I and Semi II. During the Heavy ozone pollution, the averaged OH, HO_2, and RO_2 concentrations were 1.90, 2.15, and 1.98 times higher than those in the Semi periods, suggesting a stronger oxidation capacity, with k_{OH} in Heavy being 26.43% and 9.56% higher than in Semi I and Semi II, respectively. Limited anthropogenic emissions in the suburban environment reduced the oxidation contribution by NOx and CO (27.59%). During the heavy pollution, organic species exhibited dominant behavior regarding diurnal reactivity (9.22 s^{-1} for 69.79%), and anthropogenic hydrocarbons were not major k_{OH} sources. With an abundant level (~1 ppb), isoprene contributed more than 10% of the reactivity in the diurnal cycle. Therefore, the effect of BVOCs species (such as monoterpenes, limonene, etc.) on radical chemistry cannot be ignored (Ma et al., 2022; Wang et al., 2022b). k_{OVOCs} are categorized into three groups: $k_{OVOCs(Obs)}$, $k_{OVOCs(Model)}$, and k_{HCHO}. Given the significance of formaldehyde photolysis, the contribution of HCHO to k_{OVOCs} is distinguished. $k_{OVOCs(Obs)}$ encompasses species observed in addition to formaldehyde, such as acetaldehyde (ACD) and the oxidation products of isoprene (MACR and MVK). Intermediates generated by the model, including glyoxal (GLY), methylglyoxal (MGLY), higher aldehydes (ALD), ketones (KET), methyl ethyl ketone (MEK), and methanol (MOH), are classified as $k_{OVOCs(Model)}$. Upon considering $k_{OVOCs(Model)}$ calculated by RACM2-LIM1 mechanism, the reactivity calculated prior to September 10th aligns quite well with the observed OH reactivity.

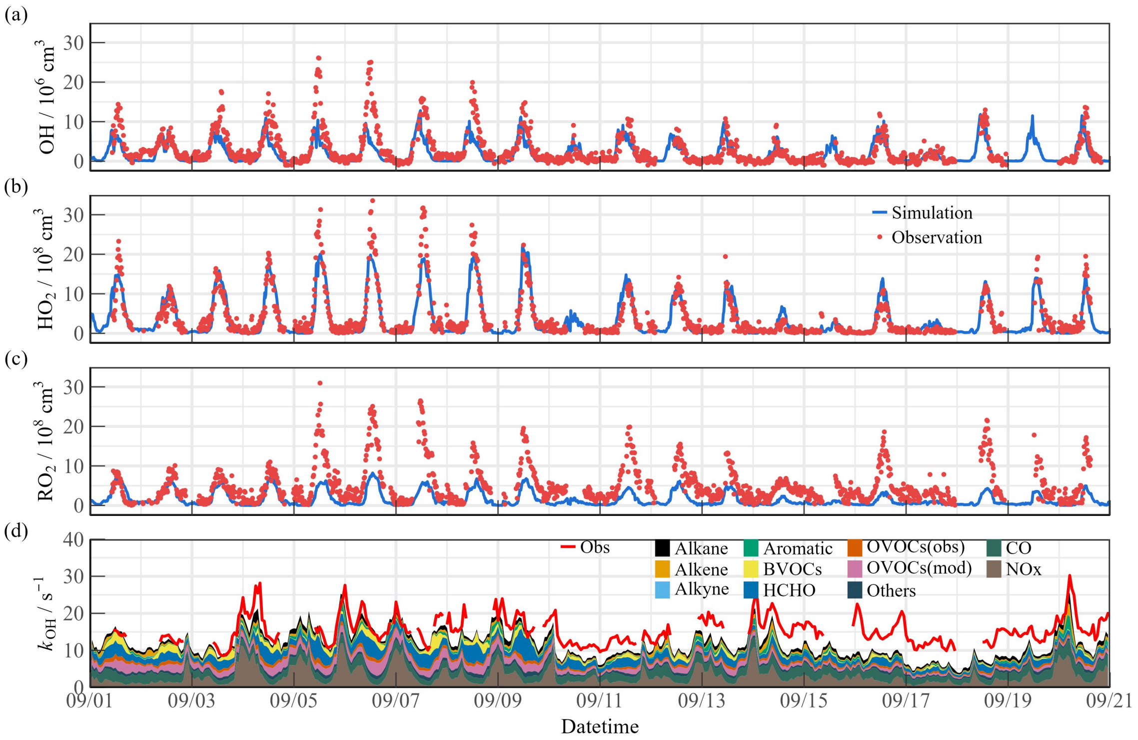

Fig. 4. Timeseries of the observed and modelled parameters for OH, HO_2 and k_{OH} during the observation period. **(a)** OH, **(b)** HO_2, **(c)** k_{OH}.

The significant variations in oxidation can be inferred from the disparities during different pollution periods (Fig. S5). During Semi I, there was a good agreement between the measurement and model for peroxy radicals during the daytime. The RACM2-LIM1 mechanism effectively replicated the morning OH radical concentration. However, following 10:00, NO gradually declined, and the increasing OH concentration could not be accounted for by the HO_2+NO formation channel, resulting in a maximum underestimation of 5.85×10^{6} cm^{-3} (Hofzumahaus et al., 2009; Lu et al., 2012). In the Semi II episode, OH was not underestimated in the low-NO regime, with a slight overestimation of HO_2 concentration. However, the simulated RO_2 concentration was only 3.78×10^{8} cm^{-3}, whereas observations were 2.77 times larger than the simulation, indicating the existence of additional reaction pathways that likely propagated the OH→RO_2 conversion efficiency. A significant discrepancy of radicals existed in the heavy ozone concentration, with OH, HO_2, and RO_2 radicals concurrently underestimated at noon by 8.23×10^{6} cm^{-3}, 3.94×10^{8} cm^{-3} and 11.59×10^{8} cm^{-3}, respectively. The observed HO_2/RO_2 ratio approached 1:1, while the model reflected an unreasonable ratio of 3:1, indicating deficiencies in both primary sources and secondary propagation. The calculated reactivity seems to compare well with the observed OH reactivity at the start of the measurement period, but then there is evidence of missing OH reactivity after September 10th (Fig. 4(d)). Due to the limitations of available instruments, this observation only measured a limited number of OVOCs species, making it difficult to accurately quantify the contribution of larger aldehydes and ketones, carboxylic acids, nitrophenols, and other multifunctional species to k_{OH} (Wang et al., 2024). Since the MCM mechanism considers more secondary formation reactions than the RACM2 mechanism, it can qualitatively assess the photochemical role of unmeasured OVOCs species in the atmosphere (Wang et al., 2022d). The additional modeled OVOCs by the MCM v3.3.1 mechanism contributed ~2.4 s^{-1} to the missing OH reactivity (Fig. S6). During Heavy period, the reactivity of more model oxidation products increased the daytime k_{OH} by about 5.1 s^{-1}. Therefore, the observed k_{OH} can serve as an upper limit for sensitivity tests, thereby the full suite of radical measurement can be performed to explore the missing oxidation properties and ozone formation (Section 4.1).

Fig. 5 displays the diurnal profiles of the ROx budget during different episodes. In Semi I, formaldehyde photolysis showed a higher contribution (38.6%), while HONO photolysis (21.0%) and ozone photolysis (24.7%) accounted for similar proportions in primary sources. The contribution of photolysis from other OVOCs was comparable to that of ozonolysis reactions (7.2% vs. 4.8%). However, in Semi II, the decreased oxidation level was attributed to lower ROx sources, despite the similar proportions. During the Heavy period, the primary sources dramatically increased (up to ~10 ppb/h), with HCHO photolysis contributing the most, alongside other sources at common levels (ranging between 1.74 – 2.66 ppb/h) in the YRD region (Ma et al., 2022). Fast HCHO oxidation dominated the radical primary source during heavy ozone pollution, which contrasts with the dominant role of HONO/O_3 in other megacities (Yang et al., 2022; Tan et al., 2017b; Yang et al., 2021a).

The radical removal rate during the daytime was generally balanced with production contributions. In the morning, owing to high NOx concentrations, radical termination was mainly dominated by OH+NO_2, OH+NO, RO_2+NO, and RO_2+NO_2. Furthermore, the formation of peroxy nitrate accounted for a certain proportion (~5%). As NOx concentrations decreased after 10:00, self-reactions in peroxy radicals became significant.

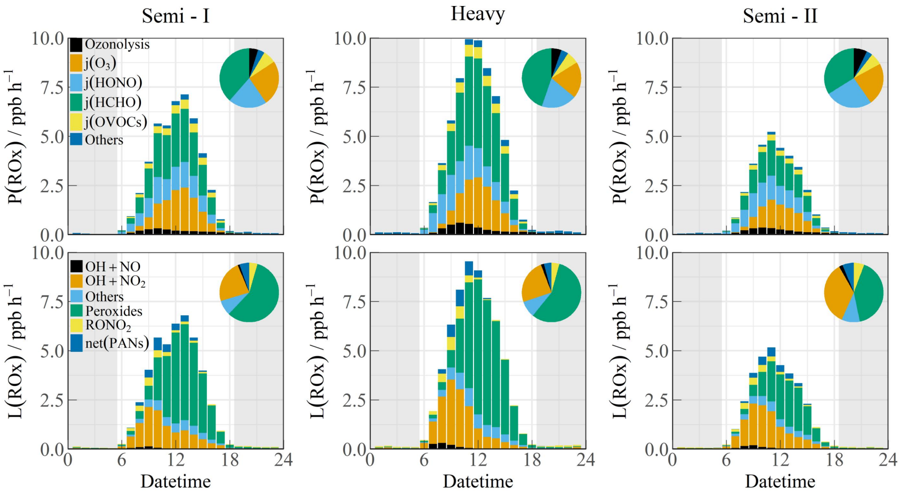

Fig. 5. The diurnal profiles of ROx budget during different polluted episodes (Semi I, Heavy, and Semi II). The pie chart denotes proportions in different parts during the daytime (10:00-15:00). The grey areas denote nighttime.

By comparing the known sources and sinks for radicals, unknown processes for initiation, transformation and termination can be determined in the experimental budget analysis (Fig. S7). During the Semi I period, the production and destruction rates of HO_2, RO_2, and total ROx radicals were very consistent, but a significant lack of a source term for OH radicals was existed after 10:00. This missing source became more pronounced during the Heavy period, reaching 16 ppb/h at noon, which is close to the results observed by APHH, but three times that observed by Heshan in PRD region(Tan et al., 2019b; Whalley et al., 2021). The ratio of OH production-to-destruction rate during the Semi II period was close to 1, indicating consistency between the observed results of OH, HO_2, k_{OH}, and other precursors(Whalley et al., 2018). However, the generation of HO_2 radicals in the morning was about twice as high as the removal rate, suggesting that there are contributions from unconsidered HO_2 radical removal channels (such as heterogeneous reactions)(Song et al., 2021). During the Heavy period, there was a rapid total removal rate of RO_2 radicals, reflecting the dominated HO_2 generation by the reaction of RO_2 radicals with NO. Although the P(HO_2) and D(HO_2) were quite in balance, the removal rate of RO_2 radicals far exceeded the known production rate (especially before 12:00). Previous work has shown that halogen chemistry (such as photolysis of nitryl chloride ($ClNO_2$)) could be an important source in the morning time, but this was not included in the calculation of ROx or RO_2 budget in this campaign(Tan et al., 2017b). The steady-state analysis for HO_2 radical in the London campaign emphasized that only by significantly reducing the observed RO_2-to-HO_2 propagation rate to just 15% could balance both P(HO_2) and D(HO_2), indicating that the RO_2-related mechanism for propagation to other radical species may not be fully understood(Whalley et al., 2018). Therefore, based on the current knowledge seems unlikely to explain the required source-sink difference of nearly 25 ppb/h in the RO_2 budget. Sensitivity analysis is needed to further infer the causes of the difference for the experimental budget analysis.

3.3 Oxidation comparison

The concentration of OH radicals during the daytime is a crucial indicator of atmospheric oxidation levels (Liu et al., 2021). Table 2 summarized radicals and related parameters for regions with similar latitudes (32.0° ± 2° N, $j(O^1D) \approx 2.5 \pm 0.5\times10^{-5}$ s^{-1}). The joint influence of solar radiation and local photochemistry resulted in megacities exhibiting intense oxidation levels in summer/autumn, characterized by OH radicals being maintained at approximately 10.0×10^6 cm^{-3} at noon. Notably, an observation in Houston revealed an OH concentration of nearly 20.0×10^6 cm^{-3}, with k_{OH} of 10 s^{-1} (Mao et al., 2010). In areas such as Los Angeles, Pasadena, and Tokyo, the propagation efficiency of radicals was restricted due to fresh anthropogenic emissions. OH concentrations were only half of those observed in other megacities, with higher inorganic-dominated k_{OH} recorded (Pasadena, ~20 s^{-1}) (George et al., 1999; Griffith et al., 2016; Yugo Kanaya et al., 2007). In the TROPSTECT observation, the observed k_{OH} exceeded the mean value at the same latitude (>15 s^{-1}). Additionally, during the Heavy episode, higher OH concentration (13.5×10^6 cm^{-3}) was found, comparable to the highest level at regions with similar latitude (Houston 2000/2006, (Mao et al., 2010)). Synchronous elevation in radical concentration and reactivity indicated a strong oxidation level in the YRD region.

The observations in the YRD region showed a stable conversion factor (OH-$j(O^1D)$) of $4\pm1 \times 10^{11}$ cm^{-3} s, which was comparable to other megacities in the PRD, NCP, and SCB regions (Ma et al., 2022; Tan et al., 2019a). The corresponding slope between OH concentration and solar radiation was used to quantify the oxidation efficiency from photolysis, and it was observed that a higher slope of 5.3×10^{11} cm^{-3} s during the Heavy period indicated an active radical chemistry. This implies that there is a strong oxidation efficiency from photolysis in the YRD region.

During summer and autumn seasons, photochemical pollution is a common occurrence, as noted by (Tan et al., 2021). Analysis of radical concentration across different regions reveals that the YRD region exhibited concentrations higher than 10^7 cm^{-3}, slightly lower than in Guangzhou in 2006 but consistent with observations in other megacities (Ma et al., 2022; Tan et al., 2017a; Lu et al., 2012; Yang et al., 2021a). Conversely, winter is characterized by haze pollution (Ma et al., 2019). An urban site in Shanghai reported a peak OH concentration of 2.6×10^6 cm^{-3}, closely resembling the 1.7 – 3.1×10^6 cm^{-3} range found in polluted winter atmospheres (Zhang et al., 2022a). Although no significant regional disparities in oxidation levels were detected in agglomerations, attention should be directed to the YRD region due to its elevated radical concentration, reactivity, and photolysis efficiency, signaling the need to investigate its role in radical chemistry.

Table 2. Summary of radical concentrations and related species concentrations at regions with similar latitude and megapolitan areas in China. All data are listed as the average in noontime (11:00~13:00).

Location	Latitude	Year	OH (10^6 cm^{-3})	k_{OH} (s^{-1})	j(O^1D) (10^{-5} s^{-1})	Slope (10^{11} cm^{-3} s)	References
Regions with similar latitude							
Los Angeles	34.1° N	Sep 1993	6.0	-	-	-	(George et al., 1999)
Nashville	36.2° N	Jun–Jul 1999	10.0	10.2	3.0	3.3[c]	(Martinez et al., 2003)
Houston	29.7° N	Aug 2000	20.0	9.0[b]	3.0	6.7[c]	(Mao et al., 2010)
Tokyo	35.6° N	Jul–Aug 2004	6.3	-	2.5	3.0	(Yugo Kanaya et al., 2007)
Houston	29.7° N	Sep 2006	15.0	11.0	3.1	5.0[c]	(Mao et al., 2010)
Pasadena	34.1° N	May-Jun 2010	4.0	20.0	2.5	1.6[c]	(Griffith et al., 2016)
Taizhou	32.6° N	May-Jun 2018	10.6	10.8[a]	2.1	4.8	(Ma et al., 2022)
Chengdu	30.7° N	Aug 2019	10.0	8.0	2.2	4.1	(Yang et al., 2021a)
TROPSTECT (Heavy)	31.9° N	Sep 2020	13.5	16.0	2.6	5.3	This work
TROPSTECT (Semi)	31.9° N	Sep 2020	7.2	14.2	2.4	3.1	This work
Regions in megapolitan areas in China							
Guangzhou (PRD)	23.5° N	Jul 2006	12.6	17.9	3.5[b]	4.5	(Lu et al., 2012)
Wangdu (NCP)	38.7° N	Jun–Jul 2014	8.3	15.0	1.8	4.5	(Tan et al., 2017b)
Beijing (NCP)	39.9° N	May–Jun 2017	9.0	30.0	2.4	3.8[c]	(Whalley et al., 2021)
Taizhou (YRD)	32.6° N	May-Jun 2018	10.6	10.8[a]	2.1	4.8	(Ma et al., 2022)
Shenzhen (PRD)	22.6° N	Sep-Oct 2018	4.5	21.0	1.8	2.4	(Yang et al., 2022)
Chengdu (SCB)	30.7° N	Aug 2019	9.0	8.0	2.2	4.0	(Yang et al., 2021a)
Hefei (YRD)	31.9° N	Sep 2020	10.4	14.3	2.4	4.4	This work

[a] The modeled k_{OH}.

[b] Value only in the afternoon.

[c] Using the ratio of OH / j(O^1D)

4 Discussion

4.1 Measurement–model reconciliation for radicals

4.1.1 OH underestimation

Full suite of OH, HO_2, RO_2 and k_{OH} was utilized in the TROPSTECT campaign to untangle a thorough understanding of oxidation mechanisms where base model failed. One specific phenomenon was the absence of an OH source in situations where NO levels gradually decreased after 10:00. Missing OH sources are closely related to the chemistry of OVOCs(Yang et al., 2024a; Qu et al., 2021). Reactive aldehyde chemistry, particularly the autoxidation of carbonyl organic peroxy radicals ($R(CO)O_2$) derived from higher aldehydes, is a significant OH regeneration mechanism that has been shown to contribute importantly to OH sources in regions with abundant natural and anthropogenic emissions during warm seasons(Yang et al., 2024b). In this study, the higher aldehyde mechanism (HAM) by Yang et al was parameterized into the base model to test new insights into the potential missing radical chemistry (Fig. 6). The results indicate that the contribution of the HAM mechanism to OH radicals in different episodes ranged between 4.4% - 6.0% (Fig. 6(a)). The additional HAM mechanism seems to have a small effect on the measured OH radical concentration. Thus, an empirical hypothesis is proposed in the 'HAM+4ALD on' scenario to increase the concentration of higher-order aldehydes by approximately fourfold, thereby replicating the effect of missing OVOCs sources on radicals. Detailed description is presented in Section 4.3.

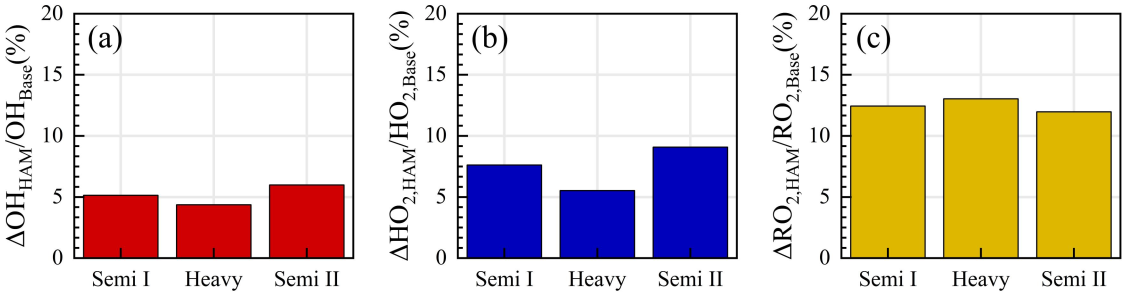

Fig. 6. The response of **(a)** OH, **(b)** HO_2 and **(c)** RO_2 radicals to the Higher Aldehyde Mechanism (HAM) in different episodes (Semi I, Heavy, and Semi II) in diurnal time (10:00-15:00).

4.1.2 RO_2 underestimation

The base scenario in Semi II is capable of accurately reproducing the concentrations of OH and HO_2 radicals within the data uncertainty. However, the simulated RO_2 concentration by the base model is only 3.78×10^{8} cm^{-3}, which does not align with the observed oxidation levels in YRD, indicating a clear discrepancy. This underestimation is similarly evident in the APHH observation in Beijing, as the highest observed concentration of RO_2 radicals reached 5.5×10^9 cm^{-3}, far exceeding the level predicted by the MCM v3.3.1 mechanism (Whalley et al., 2021). The failure to reproduce the RO_2 concentration reflects the inadequacy of the mechanisms related to RO_2 radicals due to diverse oxidation reactions. This issue is further elucidated by previous studies, which highlighted the possibility of certain VOCs undergoing more intricate isomerization or fragmentation steps to sustain the long lifetime of RO_2 radicals (Whalley et al., 2018; Whalley et al., 2021). Higher aldehyde chemistry is a concrete manifestation of verifying the aforementioned hypothesis for RO_2 sources(Yang et al., 2024b). The autoxidation process of $R(CO)O_2$, encompasses a hydrogen migration process that transforms it into the ·OOR(CO)OOH radical(Wang et al., 2019b). This radical subsequently reacts with NO to yield the ·OR(CO)OOH radical. The ·OR(CO)OOH radical predominantly undergoes two successive rapid hydrogen migration reactionss, ultimately resulting in the formation of HO_2 radicals and hydroperoxy carbonyl (HPC). Consequently, the HAM mechanism extends the lifetime of the RO_2 radical, providing a valuable complement to the unaccounted sources of RO_2 radicals. As depicted in Fig. 6, the incorporation of the HAM mechanism results in an approximate 7.4% and 12.5% increase in the concentrations of HO_2 and RO_2 radicals, respectively.

It is important to note that the total concentrations of primary emitted aldehydes and the HPC group may be underestimated, which could lead to the aforementioned analysis being conservative in nature. The union of k_{OH} and RO_2 measurement can help reveal the magnitude of missing RO_2 as a hypothesis of sensitivity analysis. Discrepancy of OH reactivity (~3 - 5 s^{-1}) between measurement and model suggested that an additional driving force was necessary to complete the OH to RO_2 step. Additional monoterpene species (MTS) was employed to represent the complex isomerization steps experienced by RO_2 radicals derived from other unmeasured VOCs. In the ‘HAM+4ALD+MTS’ scenario, approximately 0.4 ppb of monoterpenes are introduced as as the reactive BVOCs. The 0.4 ppb monoterpene level aligns with another observation from the EXPLORE-2018 campaign conducted in a suburban environment of YRD region, and can better reconcile the missing k_{OH} between observation and simulation (Fig. 7) (Wang et al., 2022b). The RACM2 mechanism identified α-pinene (API) and limonene (LIM) as representative of monoterpenes, and the mean of the species was considered the average effect of monoterpenes chemistry (the green line in Fig. 7). The 'HAM +4ALD+MTS on' scenario can reasonably reproduce the measured reactivity, and the chemistry of peroxy radicals in Semi II was reasonably described by introducing the source of complex alkoxy radicals, decreasing the obs-to-mod ratio from 2.2 to 1.3. Furthermore, the introduction of additional complex alkoxy radicals had minimal impact on HOx chemistry, with changes in daytime OH and HO_2 concentrations of less than 5×10^5 cm^{-3} and 2.5×10^7 cm^{-3}, respectively. This demonstrates the robustness of HOx radical in response to potential monoterpene.

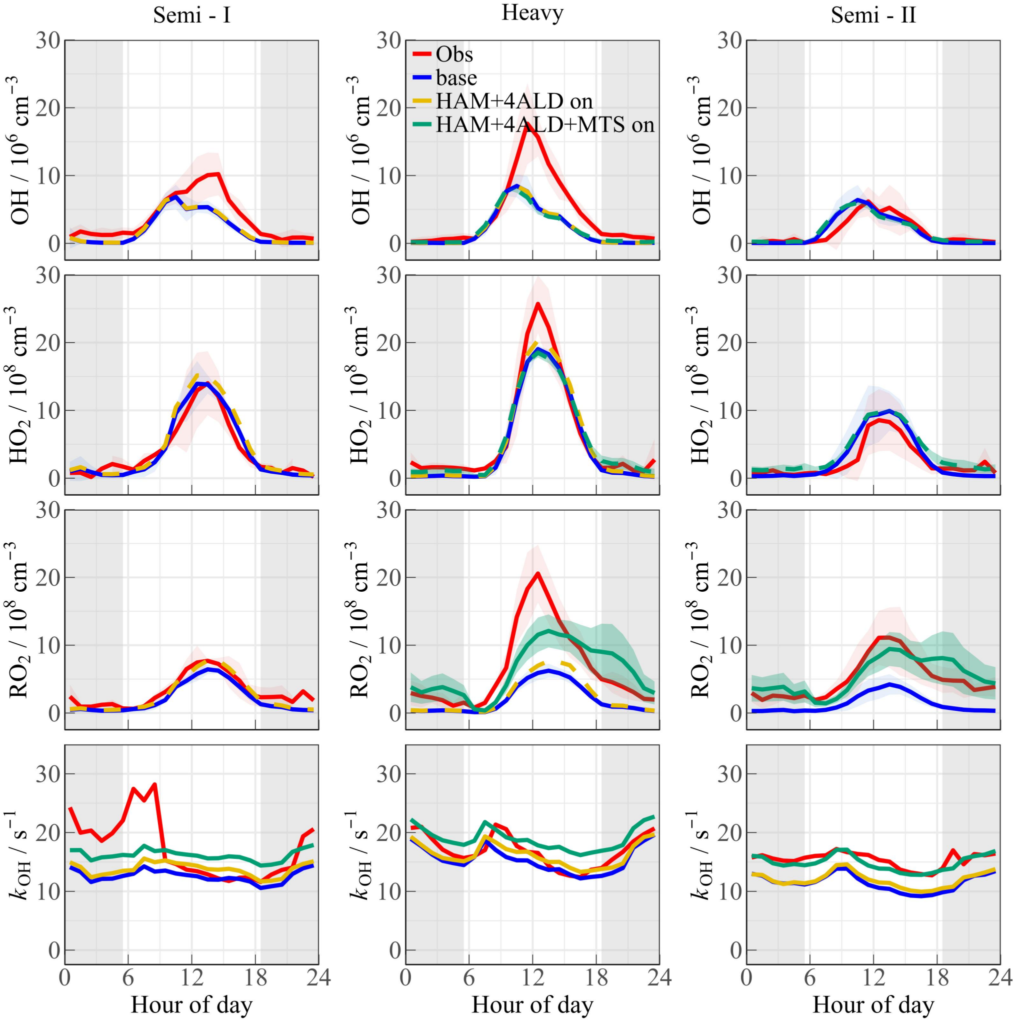

Fig. 7. The mean diurnal profiles of measured and modeled OH, HO_2, RO_2 and k_{OH} at different scenarios. Among them, the red, blue, and dotted yellow lines represent the observed values, simulated values under base model and 'HAM+4ALD' scenario, respectively. The green line and its shaded area represent the results under the 'HAM+FALD+MTS' scenario. The grey areas denote nighttime.

4.2 Effect of mechanism reconciliation on oxidation

Upon completing the hypothetical investigation into the radical underestimation, both radical concentration and oxidation coordinating deficiency are worthy of examine (Fig. S8). To eliminate the influence of non-photolytic processes, only the daytime concentration range with j(O^1D) greater than 5×10^{-6} s^{-1} was selected. The boxplots illustrate the ratio of observation to simulation (base model), with the circles representing the average values after integrating different mechanisms into the base scenario. In the low NO regime (NO < 1 ppb), the OH underestimation was consistently prominent as NO concentration decreased, and the base model was able to reasonably reflect the HO_2 distribution contrastly. As NO levels increased, the simulated OH concentration aligned well with the observation, but both HO_2 and RO_2 concentrations exhibited underprediction. RO_2 underestimation extended across the entire NO range, and could rise to over 10 times when NO levels reached about 10 ppb. Sensitivity tests based on the full suite of radical measurement revealed that the introduction of larger RO_2 alleviated the absence of certain sources by 2 to 4 times.

The coordinate ratios of radical serves as another test for ROx propagation (Fig. 8). The observed HO_2/OH ratio is approximately 100, declining to some extent as the concentration of NO increases, which is consistent with previous studies (Griffith et al., 2016; Griffith et al., 2013). However, the base model does not accurately replicate the curve depicting the change in HO_2/OH ratio, as shown in Fig. 8 (a). At low NO levels, the ratio significantly overestimated and shows a steeper decline compared to the base scenario as NO levels increase. Furthermore, the observed RO_2/OH ratios remain around 100, whereas the predicted values are significantly underestimated when NO exceeds 1 ppb (refer to Fig. 8(b)). In terms of the observed HO_2/RO_2 ratio, it maintains a relatively constant trend within the range of 0.5 – 1.5, while the model overestimated by more than twice, highlighting an inconsistency between the conversion of $RO_2 \rightarrow HO_2$. The incorporation of the HAM mechanism has proven to slightly balance the HO_2/OH ratio as illustrated in Fig. 8(a), and altered the coordination between RO_2 and OH across the entire NO range (Fig. 8(b)). The larger RO_2 isomerization associated with HAM mechanism in chemically complex environments is key to fully understanding tropospheric chemistry, and a better coordination of HO_2/OH, RO_2/OH, and HO_2/RO_2

ratios are established by incorporating additional mechanisms.

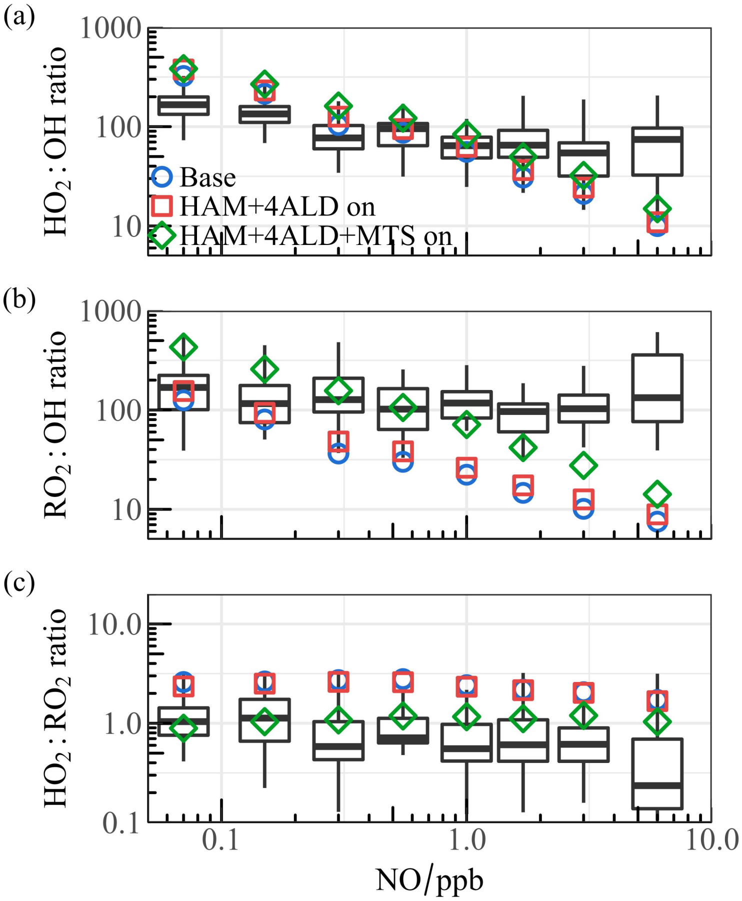

Fig. 8. The ratios for **(a)** HO_2/OH, **(b)** RO_2/OH, and **(c)** HO_2/RO_2 show a correlation with NO levels. Boxplot diagrams are used to illustrate the minimum, 25th percentile, median, 75th percentile, and maximum values of the observed dataset. The point styles (circular, square, diamond-shaped) represent the median values for the base model as well as for different mechanisms added to the model within various ranges.

The HO_2/RO_2 parameter was utilized to explore the transformation relationship between HO_2 and RO_2 radicals. If HO_2 is formed from an RO_2 radical, it would result in an HO_2/RO_2 radical concentration ratio of approximately 1. The HO_2/RO_2 ratios derived from radical concentrations measured by laser-induced fluorescence instruments and calculated using the MCM or RACM models were summarized in Fig. 9. In field studies, the observed HO_2/RO_2 ratios were between 0.2 - 1.7 under low-NO conditions (NO < 1 ppb) and only 0.1 - 0.8 under high-NO conditions (3 < NO < 6 ppb). From the perspective of model-observation matching, except for three measurements in ClearfLo, ICOZA and APHH-summer campaigns, the HO_2/RO_2 ratios in other regions could be reasonably reflected by the MCM or RACM2 mechanisms(Woodward-Massey et al., 2023; Whalley et al., 2021; Whalley et al., 2018; Färber et al., 2024). However, the ratio is generally underestimated under high NO conditions, reaching up to 5 times in ClearfLo. According to the latest chamber experiments, the HO_2/RO_2 radical concentration ratios for VOCs forming HO_2 are 0.6 for both one-step and two-step reactions. Therefore, the extremely low HO_2/RO_2 ratios observed in field campaigns can only be explained if almost all RO_2 radicals undergo multiple-step reactions before forming HO_2. During the TROPSTECT campaign, the observed HO_2/RO_2 remains at 1.1 and 0.8 under low-NO and high-NO conditions, respectively. After considering the sources of complex alkoxy radicals in the 'HAM +4ALD+MTS on' scenario, the simulated values of HO_2/RO_2 in both low-NO and high-NO regions match the observed values well.

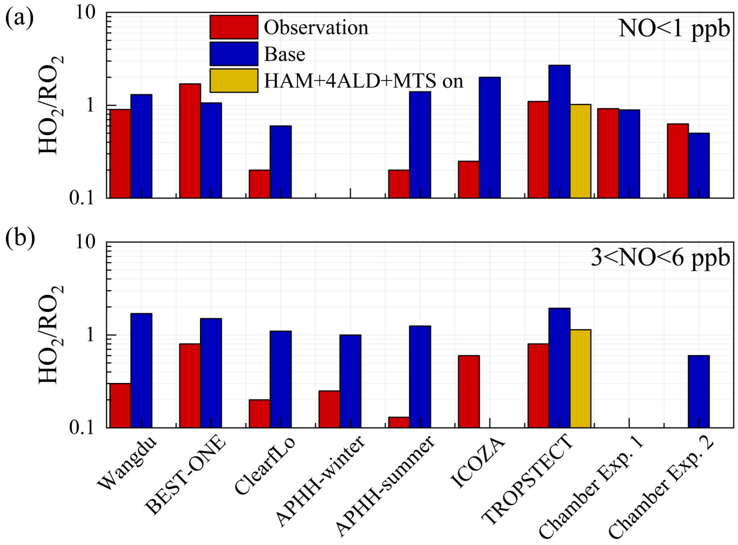

Fig. 9. Summary of the HO_2/RO_2 ratios derived from radical concentrations measured by laser-induced fluorescence instruments and calculated using the MCM or RACM models under **(a)** low-NO and **(b)** high-NO conditions. Charmber Exp. 1 and Charmber Exp. 2 denotes the parameters by single-step HO_2 formation and multi-step HO_2 formation determined in the chamber by (Färber et al., 2024).

4.3 Missing OVOCs sources influence ozone production

The consistency between model predictions and observed measurements for ozone production, akin to the concentration ratio of HO_2/RO_2, is depicted in Fig. 10(a)(b). In areas with low NO levels, the ratio of modeled to actual ozone production ranges from 0.5 to 2, with the exception of the ClearfLo and APHH-summer datasets(Woodward-Massey et al., 2023; Whalley et al., 2021). Conversely, under high NO conditions (with NO concentrations between 3 and 6 ppbv), the ozone production rate (P(Ox)) derived from measured radical concentrations typically exceeds that of the base model's predictions by more than threefold. Laboratory experiments focusing on the oxidation of representative VOCs suggest that ozone production can be enhanced by approximately 25% for the anthropogenic VOCs under investigation(Färber et al., 2024).

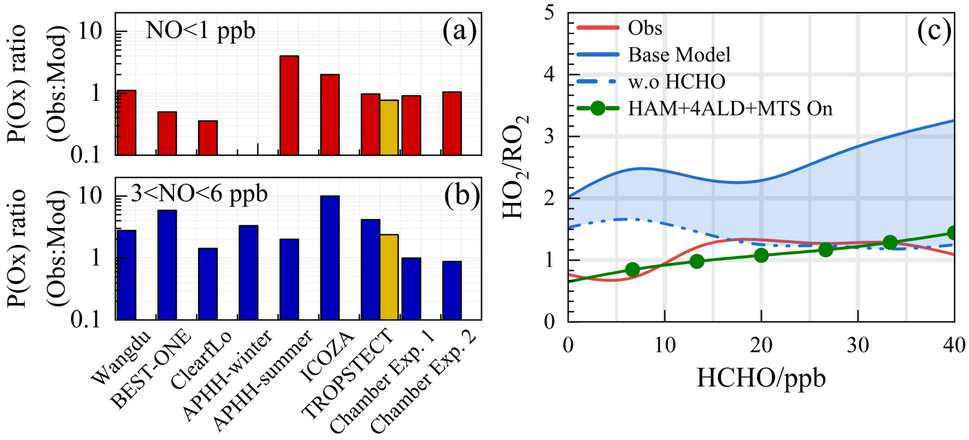

Fig. 10. Summary of the $P(Ox)_{Obs}/P(Ox)_{Mod}$ under **(a)** low-NO and **(b)** high-NO conditions. The yellow bar chart represents the simulation scenario of 'HAM +4ALD+MTS on'. **(c)** The ratios for HO_2/RO_2 show a correlation with HCHO levels. The blue shading represents the range of variation from constrained to unconstrained formaldehyde conditions. Charmber Exp. 1 and Charmber Exp. 2 denotes the parameters by single-step HO_2 formation and multi-step HO_2 formation determined in the chamber by (Färber et al., 2024).

The reasons for the discrepancy between simulated and observed values for ozone production deserve further investigation. As depicted in Fig. 10(c), the simulated HO_2/RO_2 ratios display a robust positive correlation with photochemical activity, fluctuating between 2 and 4. A notable feature during severe ozone pollution is the intense distribution of formaldehyde, with an average concentration of 21.81 ± 4.57 ppb (11:00 – 13:00). While formaldehyde acts as a precursor for HO_2 radicals, it does not directly generate RO_2 radicals. The contributions of OVOCs to the ROx radical do not exhibit the same intensity as formaldehyde, and the current mechanism encounters difficulties in replicating formaldehyde concentrations (Fig. S9). The simulation of formaldehyde concentrations using the MCM v3.3.1 mechanism has shown improvement, indicating that the secondary formation of unmeasured species, such as OVOCs, will feedback on RO_2 radical levels. When formaldehyde levels are unconstrained, the simulated HO_2/RO_2 ratios align with observations, suggesting that under the prevailing chemical mechanism, the photochemical efficiency of formaldehyde and other OVOCs is similar. Therefore, an empirical hypothesis is proposed to amplify the concentration of higher-order aldehydes by a factor of about 4, which is the proportion of formaldehyde concentration underestimated by the model. The qualitative assessment of the impact of missing aldehyde primary emissions on RO_2 radical concentrations was combined with the HAM mechanism across the entire photochemical spectrum (Fig. S10). Enhanced impact of aldehyde autoxidation in the presence of weak photochemical conditions could alter the simulated levels of OH and HO_2 radicals by approximately 13.9% and 18.1%, respectively. However, higher ALD concentrations will be achieved under intensive photochemical conditions, leading to the gradual dominance of the sink channels for OH + OVOCs, with the effect of autoxidation mechanisms gradually decreasing. RO_2 radical concentrations is notably more sensitive to the HAM mechanism, where incorporates additional OVOCs, can enhance the simulation of RO_2 radical concentrations by 20 - 40%.

On the basis of HAM mechanism, the 'HAM +4ALD+MTS on' scenario represents an effort to enhance the congruence between modeled and measured radical concentrations. In Fig. S11, with increasing NO concentration, the overall P(Ox) amplified, reaching a maximum of approximately 30 ppb/h. However, the imperfect understanding of the mechanisms related to peroxy radicals ultimately leads to misjudgment of the ozone production process in high NO regimes, with a degree of underestimation close to 10 times, as illustrated in Fig. S11(b). Notably, the deficiency in the ozone generation mechanism was adequately explained within a certain range in the 'HAM +4ALD+MTS on' scenario, leading to an enhancement in the simulation performance of P(Ox) in the high NOx region. The incorporation of OVOCs and larger alkoxy radicals derived from monoterpenes has refined the model-measurement agreement for ozone formation under high NO conditions, reducing the discrepancy from 4.17 to 2.39 (Fig. 11).

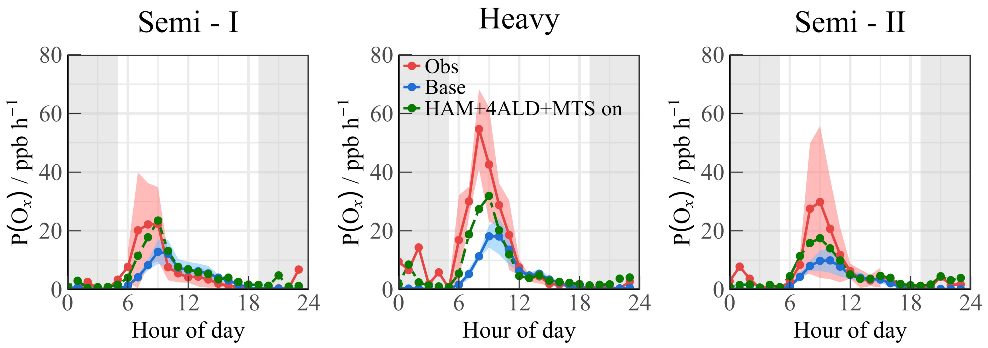
Semi - I

Heavy

Semi - II

Fig. 11. The P(Ox) values that calculated by radical values under different scenarios. The grey areas denote nighttime.

Therefore, reasonable simulation of the concentration of peroxy radicals is key to accurately quantifying the process of ozone generation. Although limiting formaldehyde can partially offset the HO_2 radical cycle and enhance the precision of HOx radical chemistry studies, additional measurements should be undertaken for other OVOCs, coupled with the deployment of full-chain radical detection systems, to accurately elucidate the oxidation processes under severe ozone pollution conditions.

5 Conclusion

The full suite radical measurement of OH, HO_2, RO_2 and k_{OH} was first deployed in the YRD region (TROPSTECT) and encountered with a prolonged ozone pollution in September 2020. The diurnal peaks of radicals exhibited considerable variation due to environmental factors, showing ranges of 3.6 to 27.1×10^6 cm^{-3} for OH, 2.1 to 33.2×10^8 cm^{-3} for HO_2, and 4.9 to 30.5×10^8 cm^{-3} for RO_2. Continuous k_{OH} data fell within a range of 8.6 – 30.2 s^{-1}, demonstrating the dominant behavior of organic species in diurnal reactivity. Furthermore, observations in the YRD region were found to be similar to those in other megacities, suggesting no significant regional differences in oxidation levels were observed in agglomerations overall.

At a heavy ozone pollution episode, the oxidation level reached intensive compared with other sites, and the simulated OH, HO_2, and RO_2 radicals provided by the RACM2-LIM1 mechanism failed to adequately match the observed data both in radical concentration and experimental radical budget. Sensitivity tests based on the full suite of radical measurement revealed that the HAM mechanism effectively complements the non-traditional regeneration of OH radicals, improving by 4.4% - 6.0% compared to the base scenario, while the concentrations of HO_2 and RO_2 radicals increased by approximately 7.4% and 12.5%, respectively. Under the constraints of k_{OH} measurement, the inclusion of OVOCs and larger alkoxy radicals derived from monoterpenes enabled better coordination of HO_2/OH, RO_2/OH, and HO_2/RO_2 ratios, and adequately improved the model-measurement consistency for ozone formation, reducing the discrepancy under high NO conditions from 4.17 to 2.39. This study enabled a deeper understanding of the tropospheric radical chemistry at play. Notably,

- ✓ A full suite of radical measurement can untangle the gap-bridge for the base model in more chemically-complex environments as an hypothesis of sensitivity tests.

- ✓ Additional measurements targeting more OVOCs should also be conducted to fulfill the RO_2-related imbalance, and then accurately elucidating the oxidation under severe ozone pollution.

Financial support

This work was supported by the National Key R&D Program of China (2022YFC3700301), the National Natural Science Foundation of China (62275250, U19A2044, 42030609), the Natural Science Foundation of Anhui Province (No. 2008085J20), the Anhui Provincial Key R&D Program (2022l07020022), and the Distinguished Program of Jianghuai Talents Program of Excellence (HYRCSTZ202401).

Data availability

The data used in this study are available upon request (rzhu@aiofm.ac.cn).

Author contributions

WQ Liu, PH Xie, RZ Hu contributed to the conception of this study. RZ Hu and GX Zhang performed the data analyses and manuscript writing. All authors contributed to measurements, discussed results, and commented on the paper.

Competing interests

The contact author has declared that none of the authors has any competing interests.

References

Duan, J., Qin, M., Ouyang, B., Fang, W., Li, X., Lu, K., Tang, K., Liang, S., Meng, F., Hu, Z., Xie, P., Liu, W., and Häsler, R.: Development of an incoherent broadband cavity-enhanced absorption spectrometer for in situ measurements of HONO and NO_2, Atmos Meas Tech, 11, 4531-4543, 10.5194/amt-11-4531-2018, 2018.

Färber, M., Fuchs, H., Bohn, B., Carlsson, P. T. M., Gkatzelis, G. I., Marcillo Lara, A. C., Rohrer, F., Vereecken, L., Wedel, S., Wahner, A., and Novelli, A.: Effect of the Alkoxy Radical Chemistry on the Ozone Formation from Anthropogenic Organic Compounds Investigated in Chamber Experiments, ACS ES&T Air, 1, 1096-1111, 10.1021/acsestair.4c00064, 2024.

Fuchs, H., Holland, F., and Hofzumahaus, A.: Measurement of tropospheric RO_2 and HO_2 radicals by a laser-induced fluorescence instrument, Rev of Sci Inst, 79, 084104, 10.1063/1.2968712, 2008.

George, L. A., Hard, T. M., and O'Brien, R. J.: Measurement of free radicals OH and HO_2 in Los Angeles smog, J Geophys Res-Atmos, 104, 11643-11655, 1999.

Griffith, S. M., Hansen, R. F., Dusanter, S., Stevens, P. S., Alaghmand, M., Bertman, S. B., Carroll, M. A., Erickson, M., Galloway, M., Grossberg, N., Hottle, J., Hou, J., Jobson, B. T., Kammrath, A., Keutsch, F. N., Lefer, B. L., Mielke, L. H., O'Brien, A., Shepson, P. B., Thurlow, M., Wallace, W., Zhang, N., and Zhou, X. L.: OH and HO_2 radical chemistry during PROPHET 2008 and CABINEX 2009-Part 1: Measurements and model comparison, Atmos Chem Phys, 13, 5403-5423, 10.5194/acp-13-5403-2013, 2013.

Griffith, S. M., Hansen, R. F., Dusanter, S., Michoud, V., Gilman, J. B., Kuster, W. C., Veres, P. R., Graus, M., de Gouw, J. A., Roberts, J., Young, C., Washenfelder, R., Brown, S. S., Thalman, R., Waxman, E., Volkamer, R., Tsai, C., Stutz, J., Flynn, J. H., Grossberg, N., Lefer, B., Alvarez, S. L., Rappenglueck, B., Mielke, L. H., Osthoff, H. D., and Stevens, P. S.: Measurements of hydroxyl and hydroperoxy radicals during CalNex-LA: Model comparisons and radical budgets, J Geophys Res-Atmos, 121, 4211-4232, 10.1002/2015jd024358, 2016.

Heard, D. E. and Pilling, M. J.: Measurement of OH and HO_2 in the troposphere, Chemical reviews, 103, 5163-5198, 10.1021/cr020522s, 2003.

Hofzumahaus, A., Rohrer, F., Lu, K., Bohn, B., Brauers, T., Chang, C.-C., Fuchs, H., Holland, F., Kita, K., Kondo, Y., Li, X., Lou, S., Shao, M., Zeng, L., Wahner, A., and Zhang, Y.: Amplified Trace Gas Removal in the Troposphere, Science, 324, 1702-1704, 10.1126/science.1164566, 2009.

Hu, B., Duan, J., Hong, Y., Xu, L., Li, M., Bian, Y., Qin, M., Fang, W., Xie, P., and Chen, J.: Exploration of the atmospheric chemistry of nitrous acid in a coastal city of southeastern China: results from measurements across four seasons, Atmos Chem Phys, 22, 371-393, 10.5194/acp-22-371-2022, 2022.

Huang, J., Pan, X., Guo, X., and Li, G.: Health impact of China's Air Pollution Prevention and Control Action Plan: an analysis of national air quality monitoring and mortality data, Lancet Planet Health, 2, e313-e323, 10.1016/S2542-5196(18)30141-4, 2018.

Huang, X., Ding, A., Wang, Z., Ding, K., Gao, J., Chai, F., and Fu, C.: Amplified transboundary transport of haze by aerosol–boundary layer interaction in China, Nature Geoscience, 13, 428-434, 10.1038/s41561-020-0583-4, 2020.

Jenkin, M. E., Saunders, S. M., and Pilling, M. J.: The tropospheric degradation of volatile organic compounds: A protocol for mechanism development, Atmos Environ, 31, 81-104, 10.1016/s1352-2310(96)00105-7, 1997.

Jenkin, M. E., Saunders, S. M., Wagner, V., and Pilling, M. J.: Protocol for the development of the Master Chemical Mechanism, MCM v3 (Part B): tropospheric degradation of aromatic volatile organic compounds, Atmos Chem Phys, 3, 181-193, 10.5194/acp-3-181-2003, 2003.

Jia, W., Zhang, X., and Wang, Y.: Assessing the pollutant evolution mechanisms of heavy pollution episodes in the Yangtze-Huaihe valley: A multiscale perspective, Atmos Environ, 244, 10.1016/j.atmosenv.2020.117986, 2021.

Kanaya, Y., Hofzumahaus, A., Dorn, H. P., Brauers, T., Fuchs, H., Holland, F., Rohrer, F., Bohn, B., Tillmann, R., Wegener, R., Wahner, A., Kajii, Y., Miyamoto, K., Nishida, S., Watanabe, K., Yoshino, A., Kubistin, D., Martinez, M., Rudolf, M., Harder, H., Berresheim, H., Elste, T., Plass-Duelmer, C., Stange, G., Kleffmann, J., Elshorbany, Y., and Schurath, U.: Comparisons of observed and modeled OH and HO_2 concentrations during the ambient measurement period of the HO(x)Comp field campaign, Atmos Chem Phys, 12, 2567-2585, 10.5194/acp-12-2567-2012, 2012.

Levy, H.: Normal Atmosphere: Large Radical and Formaldehyde Concentrations Predicted, Science, 173, 141-143, 10.1126/science.173.3992.141, 1971.

Li, S., Lu, K., Ma, X., Yang, X., Chen, S., and Zhang, Y.: Field measurement of the organic peroxy radicals by the low-pressure reactor plus laser-induced fluorescence spectroscopy, Chinese Chemical Letters, 31, 2799-2802, 10.1016/j.cclet.2020.07.051, 2020.

Liu, S., Li, X., Shen, X., Zeng, L., Huang, X., Zhu, B., Lin, L., and Lou, S.: Measurement and partition analysis of atmospheric OH reactivity in autumn in Shenzhen, Acta Scientiae Circumstantiae, 39, 3600-3610, 2019.

Liu, Y., Li, J., Ma, Y., Zhou, M., Tan, Z., Zeng, L., Lu, K., and Zhang, Y.: A review of gas-phase chemical mechanisms commonly used in atmospheric chemistry modelling, Journal of Environmental Sciences, 10.1016/j.jes.2022.10.031, 2022.

Liu, Z., Wang, Y., Hu, B., Lu, K., Tang, G., Ji, D., Yang, X., Gao, W., Xie, Y., Liu, J., Yao, D., Yang, Y., and Zhang, Y.: Elucidating the quantitative characterization of atmospheric oxidation capacity in Beijing, China, Sci Total Environ, 771, 10.1016/j.scitotenv.2021.145306, 2021.

Lou, S., Holland, F., Rohrer, F., Lu, K., Bohn, B., Brauers, T., Chang, C. C., Fuchs, H., Haseler, R., Kita, K., Kondo, Y., Li, X., Shao, M., Zeng, L., Wahner, A., Zhang, Y., Wang, W., and Hofzumahaus, A.: Atmospheric OH reactivities in the Pearl River Delta – China in summer 2006: measurement and model results, Atmos Chem Phys, 10, 11243–11260, 10.5194/acp-10-11243-2010, 2010.

Lu, K., Guo, S., Tan, Z., Wang, H., Shang, D., Liu, Y., Li, X., Wu, Z., Hu, M., and Zhang, Y.: Exploring atmospheric free-radical chemistry in China: the self-cleansing capacity and the formation of secondary air pollution, Natl. Sci. Rev., 6, 579-594, 10.1093/nsr/nwy073, 2019a.

Lu, K. D., Guo, S., Tan, Z. F., Wang, H. C., Shang, D. J., Liu, Y. H., Li, X., Wu, Z. J., Hu, M., and Zhang, Y. H.: Exploring atmospheric free-radical chemistry in China: the self-cleansing capacity and the formation of secondary air pollution, Natl. Sci. Rev., 6, 579-594, 10.1093/nsr/nwy073, 2019b.

Lu, K. D., Rohrer, F., Holland, F., Fuchs, H., Bohn, B., Brauers, T., Chang, C. C., Haeseler, R., Hu, M., Kita, K., Kondo, Y., Li, X., Lou, S. R., Nehr, S., Shao, M., Zeng, L. M., Wahner, A., Zhang, Y. H., and Hofzumahaus, A.: Observation and modelling of OH and HO_2 concentrations in the Pearl River Delta 2006: a missing OH source in a VOC rich atmosphere, Atmos Chem Phys, 12, 1541-1569, 10.5194/acp-12-1541-2012, 2012.

Ma, X., Tan, Z., Lu, K., Yang, X., Chen, X., Wang, H., Chen, S., Fang, X., Li, S., Li, X., Liu, J., Liu, Y., Lou, S., Qiu, W., Wang, H., Zeng, L., and Zhang, Y.: OH and HO_2 radical chemistry at a suburban site during the EXPLORE-YRD campaign in 2018, Atmos Chem Phys, 22, 7005-7028, 10.5194/acp-22-7005-2022, 2022.

Ma, X. F., Tan, Z. F., Lu, K. D., Yang, X. P., Liu, Y. H., Li, S. L., Li, X., Chen, S. Y., Novelli, A., Cho, C. M., Zeng, L. M., Wahner, A., and Zhang, Y. H.: Winter photochemistry in Beijing: Observation and model simulation of OH and HO_2 radicals at an urban site, Sci Total Environ, 685, 85-95, 10.1016/j.scitotenv.2019.05.329, 2019.

Mao, J., Ren, X., Chen, S., Brune, W. H., Chen, Z., Martinez, M., Harder, H., Lefer, B., Rappenglück, B., Flynn, J., and Leuchner, M.: Atmospheric oxidation capacity in the summer of Houston 2006: Comparison with summer measurements in other metropolitan studies, Atmos Environ, 44, 4107-4115, 10.1016/j.atmosenv.2009.01.013, 2010.

Martinez, M., Harder, H., Kovacs, T. A., Simpas, J. B., Bassis, J., Lesher, R., Brune, W. H., Frost, G. J., Williams, E. J., Stroud, C. A., Jobson, B. T., Roberts, J. M., Hall, S. R., Shetter, R. E., Wert, B., Fried, A., Alicke, B., Stutz, J., Young, V. L., White, A. B., and Zamora, R. J.: OH and HO_2 concentrations, sources, and loss rates during the Southern Oxidants Study in Nashville, Tennessee, summer 1999, J Geophys Res-Atmos, 108, 10.1029/2003jd003551, 2003.

Peeters, J., Muller, J. F., Stavrakou, T., and Nguyen, V. S.: Hydroxyl Radical Recycling in Isoprene Oxidation Driven by Hydrogen Bonding and Hydrogen Tunneling: The Upgraded LIM1 Mechanism, J Phys Chem A, 118, 8625-8643, 10.1021/jp5033146, 2014.

Qu, H., Wang, Y., Zhang, R., Liu, X., Huey, L. G., Sjostedt, S., Zeng, L., Lu, K., Wu, Y., Shao, M., Hu, M., Tan, Z., Fuchs, H., Broch, S., Wahner, A., Zhu, T., and Zhang, Y.: Chemical Production of Oxygenated Volatile Organic Compounds Strongly Enhances Boundary-Layer Oxidation Chemistry and Ozone Production, Environ Sci Technol, 10.1021/acs.est.1c04489, 2021.

Ren, X., Olson, J. R., Crawford, J. H., Brune, W. H., Mao, J., Long, R. B., Chen, Z., Chen, G., Avery, M. A., Sachse, G. W., Barrick, J. D., Diskin, G. S., Huey, L. G., Fried, A., Cohen, R. C., Heikes, B., Wennberg, P. O., Singh, H. B., Blake, D. R., and Shetter, R. E.: HOx chemistry during INTEX-A 2004: Observation, model calculation, and comparison with previous studies, J Geophys Res-Atmos, 113, 10.1029/2007jd009166, 2008.

Rohrer, F., Lu, K., Hofzumahaus, A., Bohn, B., Brauers, T., Chang, C.-C., Fuchs, H., Haeseler, R., Holland, F., Hu, M., Kita, K., Kondo, Y., Li, X., Lou, S., Oebel, A., Shao, M., Zeng, L., Zhu, T., Zhang, Y., and Wahner, A.: Maximum efficiency in the hydroxyl-radical-based self-cleansing of the troposphere, Nature Geoscience, 7, 559-563, 10.1038/ngeo2199, 2014.

Shi, X., Ge, Y., Zheng, J., Ma, Y., Ren, X., and Zhang, Y.: Budget of nitrous acid and its impacts on atmospheric oxidative capacity at an urban site in the central Yangtze River Delta region of China, Atmos Environ, 238, 10.1016/j.atmosenv.2020.117725, 2020.

Slater, E. J., Whalley, L. K., Woodward-Massey, R., Ye, C., Lee, J. D., Squires, F., Hopkins, J. R., Dunmore, R. E., Shaw, M., Hamilton, J. F., Lewis, A. C., Crilley, L. R., Kramer, L., Bloss, W., Vu, T., Sun, Y., Xu, W., Yue, S., Ren, L., Acton, W. J. F., Hewitt, C. N., Wang, X., Fu, P., and Heard, D. E.: Elevated levels of OH observed in haze events during wintertime in central Beijing, Atmos Chem Phys, 20, 14847-14871, 10.5194/acp-20-14847-2020, 2020.

Song, H., Lu, K., Dong, H., Tan, Z., Chen, S., Zeng, L., and Zhang, Y.: Reduced Aerosol Uptake of Hydroperoxyl Radical May Increase the Sensitivity of Ozone Production to Volatile Organic Compounds, Environmental Science & Technology Letters, 9, 22-29, 10.1021/acs.estlett.1c00893, 2021.

Stockwell, W. R., Kirchner, F., Kuhn, M., and Seefeld, S.: A new mechanism for regional atmospheric chemistry modeling, J Geophys Res-Atmos, 102, 25847-25879, 10.1029/97jd00849, 1997.

Stone, D., Whalley, L. K., and Heard, D. E.: Tropospheric OH and HO_2 radicals: field measurements and model comparisons, Chemical Society reviews, 41, 6348-6404, 10.1039/c2cs35140d, 2012.

Tan, Z., Ma, X., Lu, K., Jiang, M., Zou, Q., Wang, H., Zeng, L., and Zhang, Y.: Direct evidence of local photochemical production driven ozone episode in Beijing: A case study, Sci Total Environ, 800, 148868, 10.1016/j.scitotenv.2021.148868, 2021.

Tan, Z., Lu, K., Jiang, M., Su, R., Wang, H., Lou, S., Fu, Q., Zhai, C., Tan, Q., Yue, D., Chen, D., Wang, Z., Xie, S., Zeng, L., and Zhang, Y.: Daytime atmospheric oxidation capacity in four Chinese megacities during the photochemically polluted season: a case study based on box model simulation, Atmos Chem Phys, 19, 3493-3513, 10.5194/acp-19-3493-2019, 2019a.

Tan, Z., Fuchs, H., Lu, K., Hofzumahaus, A., Bohn, B., Broch, S., Dong, H., Gomm, S., Haeseler, R., He, L., Holland, F., Li, X., Liu, Y., Lu, S., Rohrer, F., Shao, M., Wang, B., Wang, M., Wu, Y., Zeng, L., Zhang, Y., Wahner, A., and Zhang, Y.: Radical chemistry at a rural site (Wangdu) in the North China Plain: observation and model calculations of OH, HO_2 and RO_2 radicals, Atmos Chem Phys, 17, 663-690, 10.5194/acp-17-663-2017, 2017a.

Tan, Z. F., Lu, K. D., Dong, H. B., Hu, M., Li, X., Liu, Y. H., Lu, S. H., Shao, M., Su, R., Wang, H. C., Wu, Y. S., Wahner, A., and Zhang, Y. H.: Explicit diagnosis of the local ozone production rate and the ozone-NOx-VOC sensitivities, Sci. Bull., 63, 1067-1076, 10.1016/j.scib.2018.07.001, 2018.

Tan, Z. F., Lu, K. D., Hofzumahaus, A., Fuchs, H., Bohn, B., Holland, F., Liu, Y. H., Rohrer, F., Shao, M., Sun, K., Wu, Y. S., Zeng, L. M., Zhang, Y. S., Zou, Q., Kiendler-Scharr, A., Wahner, A., and Zhang, Y. H.: Experimental budgets of OH, HO_2, and RO_2 radicals and implications for ozone formation in the Pearl River Delta in China 2014, Atmos Chem Phys, 19, 7129-7150, 10.5194/acp-19-7129-2019, 2019b.

Tan, Z. F., Fuchs, H., Lu, K. D., Hofzumahaus, A., Bohn, B., Broch, S., Dong, H. B., Gomm, S., Haseler, R., He, L. Y., Holland, F., Li, X., Liu, Y., Lu, S. H., Rohrer, F., Shao, M., Wang, B. L., Wang, M., Wu, Y. S., Zeng, L. M., Zhang, Y. S., Wahner, A., and Zhang, Y. H.: Radical chemistry at a rural site (Wangdu) in the North China Plain: observation and model calculations of OH, HO_2 and RO_2 radicals, Atmos Chem Phys, 17, 663-690, 10.5194/acp-17-663-2017, 2017b.

Wang, F., Hu, R., Xie, P., Wang, Y., Chen, H., Zhang, G., and Liu, W.: Calibration source for OH radical based on synchronous photolysis, Acta Phys Sin-Ch Ed, 69, 2020.

Wang, F. Y., Hu, R. Z., Chen, H., Xie, P. H., Wang, Y. H., Li, Z. Y., Jin, H. W., Liu, J. G., and Liu, W. Q.: Development of a field system for measurement of tropospheric OH radical using laser-induced fluorescence technique, Opt. Express, 27, A419-A435, 10.1364/oe.27.00a419, 2019a.

Wang, H., Lu, K., Tan, Z., Chen, X., Liu, Y., and Zhang, Y.: Formation mechanism and control strategy for particulate nitrate in China, Journal of Environmental Sciences, 10.1016/j.jes.2022.09.019, 2022a.

Wang, H., Ma, X., Tan, Z., Wang, H., Chen, X., Chen, S., Gao, Y., Liu, Y., Liu, Y., Yang, X., Yuan, B., Zeng, L., Huang, C., Lu, K., and Zhang, Y.: Anthropogenic monoterpenes aggravating ozone pollution, Natl. Sci. Rev., 9, 2022b.

Wang, S.-n., Wu, R.-r., and Wang, L.-m.: Role of Hydrogen Migrations in Carbonyl Peroxy Radicals in the Atmosphere, Chinese J Chem Phys, 32, 457-466, 10.1063/1674-0068/cjcp1811265, 2019b.

Wang, T., Xue, L., Feng, Z., Dai, J., Zhang, Y., and Tan, Y.: Ground-level ozone pollution in China: a synthesis of recent findings on influencing factors and impacts, Environmental Research Letters, 10.1088/1748-9326/ac69fe, 2022c.

Wang, W., Yuan, B., Su, H., Cheng, Y., Qi, J., Wang, S., Song, W., Wang, X., Xue, C., Ma, C., Bao, F., Wang, H., Lou, S., and Shao, M.: A large role of missing volatile organic compound reactivity from anthropogenic emissions in ozone pollution regulation, Atmos Chem Phys, 24, 4017-4027, 10.5194/acp-24-4017-2024, 2024.

Wang, W., Yuan, B., Peng, Y., Su, H., Cheng, Y., Yang, S., Wu, C., Qi, J., Bao, F., Huangfu, Y., Wang, C., Ye, C., Wang, Z., Wang, B., Wang, X., Song, W., Hu, W., Cheng, P., Zhu, M., Zheng, J., and Shao, M.: Direct observations indicate photodegradable oxygenated volatile organic compounds (OVOCs) as larger contributors to radicals and ozone production in the atmosphere, Atmos Chem Phys, 22, 4117-4128, 10.5194/acp-22-4117-2022, 2022d.

Wang, Y., Hu, R., Xie, P., Chen, H., Wang, F., Liu, X., Liu, J., and Liu, W.: Measurement of tropospheric HO_2 radical using fluorescence assay by gas expansion with low interferences, J Environ Sci (China), 99, 40-50, 10.1016/j.jes.2020.06.010, 2021.

Whalley, L. K., Blitz, M. A., Desservettaz, M., Seakins, P. W., and Heard, D. E.: Reporting the sensitivity of laser-induced fluorescence instruments used for HO_2 detection to an interference from RO_2 radicals and introducing a novel approach that enables HO_2 and certain RO_2 types to be selectively measured, Atmos Meas Tech, 6, 3425-3440, 10.5194/amt-6-3425-2013, 2013.

Whalley, L. K., Stone, D., Dunmore, R., Hamilton, J., Hopkins, J. R., Lee, J. D., Lewis, A. C., Williams, P., Kleffmann, J., Laufs, S., Woodward-Massey, R., and Heard, D. E.: Understanding in situ ozone production in the summertime through radical observations and modelling studies during the Clean air for London project (ClearfLo), Atmos Chem Phys, 18, 2547-2571, 10.5194/acp-18-2547-2018, 2018.

Whalley, L. K., Slater, E. J., Woodward-Massey, R., Ye, C., Lee, J. D., Squires, F., Hopkins, J. R., Dunmore, R. E., Shaw, M., Hamilton, J. F., Lewis, A. C., Mehra, A., Worrall, S. D., Bacak, A., Bannan, T. J., Coe, H., Percival, C. J., Ouyang, B., Jones, R. L., Crilley, L. R., Kramer, L. J., Bloss, W. J., Vu, T., Kotthaus, S., Grimmond, S., Sun, Y., Xu, W., Yue, S., Ren, L., Acton, W. J. F., Hewitt, C. N., Wang, X., Fu, P., and Heard, D. E.: Evaluating the sensitivity of radical chemistry and ozone formation to ambient VOCs and NOx in Beijing, Atmos Chem Phys, 21, 2125-2147, 10.5194/acp-21-2125-2021, 2021.

Woodward-Massey, R., Sommariva, R., Whalley, L. K., Cryer, D. R., Ingham, T., Bloss, W. J., Ball, S. M., Cox, S., Lee, J. D., Reed, C. P., Crilley, L. R., Kramer, L. J., Bandy, B. J., Forster, G. L., Reeves, C. E., Monks, P. S., and Heard, D. E.: Radical chemistry and ozone production at a UK coastal receptor site, Atmos Chem Phys, 23, 14393-14424, 10.5194/acp-23-14393-2023, 2023.

Yang, X., Li, Y., Ma, X., Tan, Z., Lu, K., and Zhang, Y.: Unclassical Radical Generation Mechanisms in the Troposphere: A Review, Environ Sci Technol, 10.1021/acs.est.4c00742, 2024a.

Yang, X., Lu, K., Ma, X., Gao, Y., Tan, Z., Wang, H., Chen, X., Li, X., Huang, X., He, L., Tang, M., Zhu, B., Chen, S., Dong, H., Zeng, L., and Zhang, Y.: Radical chemistry in the Pearl River Delta: observations and modeling of OH and HO_2 radicals in Shenzhen in 2018, Atmos Chem Phys, 22, 12525-12542, 10.5194/acp-22-12525-2022, 2022.

Yang, X., Wang, H., Lu, K., Ma, X., Tan, Z., Long, B., Chen, X., Li, C., Zhai, T., Li, Y., Qu, K., Xia, Y., Zhang, Y., Li, X., Chen, S., Dong, H., Zeng, L., and Zhang, Y.: Reactive aldehyde chemistry explains the missing source of hydroxyl radicals, Nat Commun, 15, 1648, 10.1038/s41467-024-45885-w, 2024b.

Yang, X., Lu, K., Ma, X., Liu, Y., Wang, H., Hu, R., Li, X., Lou, S., Chen, S., Dong, H., Wang, F., Wang, Y., Zhang, G., Li, S., Yang, S., Yang, Y., Kuang, C., Tan, Z., Chen, X., Qiu, P., Zeng, L., Xie, P., and Zhang, Y.: Observations and modeling of OH and HO_2 radicals in Chengdu, China in summer 2019, The Science of the total environment, 772, 144829-144829, 10.1016/j.scitotenv.2020.144829, 2021a.

Yang, Y., Li, X., Zu, K., Lian, C., Chen, S., Dong, H., Feng, M., Liu, H., Liu, J., Lu, K., Lu, S., Ma, X., Song, D., Wang, W., Yang, S., Yang, X., Yu, X., Zhu, Y., Zeng, L., Tan, Q., and Zhang, Y.: Elucidating the effect of HONO on O_3 pollution by a case study in southwest China, Sci Total Environ, 756, 144127, 10.1016/j.scitotenv.2020.144127, 2021b.

Yugo Kanaya, Renqiu Cao, Hajime Akimoto, Masato Fukuda, Yuichi Komazaki, Yoko Yokouchi, Makoto Koike, Hiroshi Tanimoto, Nobuyuki Takegawa, and Kondo, a. Y.: Urban photochemistry in central Tokyo: 1. Observed and modeled OH and HO_2 radical concentrations during the winter and summer of 2004, J Geophys Res-Atmos, 112, 20, 10.1029/2007JD008670, 2007.

Yugo Kanaya, R. C., Shungo Kato, Yuko Miyakawa, Yoshizumi Kajii, Hiroshi and Tanimoto, Y. Y., Michihiro Mochida, Kimitaka Kawamura, Hajime Akimoto: Chemistry of OH and HO_2 radicals observed at Rishiri Island, Japan, in September 2003: Missing daytime sink of HO_2 and positive nighttime correlations with monoterpenes, J Geophys Res-Atmos, 112, 10.1029/2006id007987, 2007.

Zhang, G., Hu, R., Xie, P., Lou, S., Wang, F., Wang, Y., Qin, M., Li, X., Liu, X., Wang, Y., and Liu, W.: Observation and simulation of HOx radicals in an urban area in Shanghai, China, Sci Total Environ, 810, 152275, 10.1016/j.scitotenv.2021.152275, 2022a.

Zhang, G., Hu, R., Xie, P., Lu, K., Lou, S., Liu, X., Li, X., Wang, F., Wang, Y., Yang, X., Cai, H., Wang, Y., and Liu, W.: Intercomparison of OH radical measurement in a complex atmosphere in Chengdu, China, Sci Total Environ, 155924, 10.1016/j.scitotenv.2022.155924, 2022b.